SUPPORTING INFORMATION

"THE INTRINSIC LUMINESCENCE OF INDIVIDUAL PLASMONIC NANOSTRUCTURES IN AQUEOUS SUSPENSION BY PHOTON TIME-OF-FLIGHT SPECTROSCOPY"

Matthieu Loumaigne,[a,f] *Julien R. G. Navarro*,[b,‡] *Stéphane Parola*,[b]

Martinus H. V. Werts[a] *and Anne Débarre*[c]*

[a] École normale supérieure de Rennes, CNRS, SATIE (UMR8029), Campus de Ker Lann, F-35170 Bruz, France

[b] École normale supérieure de Lyon, CNRS, Univ. Lyon 1, Laboratoire de Chimie (UMR 5182) F-69364, Lyon, France

[c] Laboratoire Aimé Cotton (UMR 9188), CNRS, Univ. Paris-Sud, F-91405 Orsay, France and

PPSM (UMR 8531), CNRS, Institut d'Alembert, École normale supérieure de Cachan, F-94235 Cachan, France.

*: CORRESPONDING AUTHOR Tel: +33-1-47-40-74-43. E-mail: anne.debarre@lac.u-psud.fr.

[f]: present address: MOLTECH Anjou (UMR6200), Univ. Angers, CNRS, F-49045 Angers, France

‡ present address: Arrhenius Laboratory, Department of Materials and Environmental chemistry, Stockholm University, Stockholm, Sweden

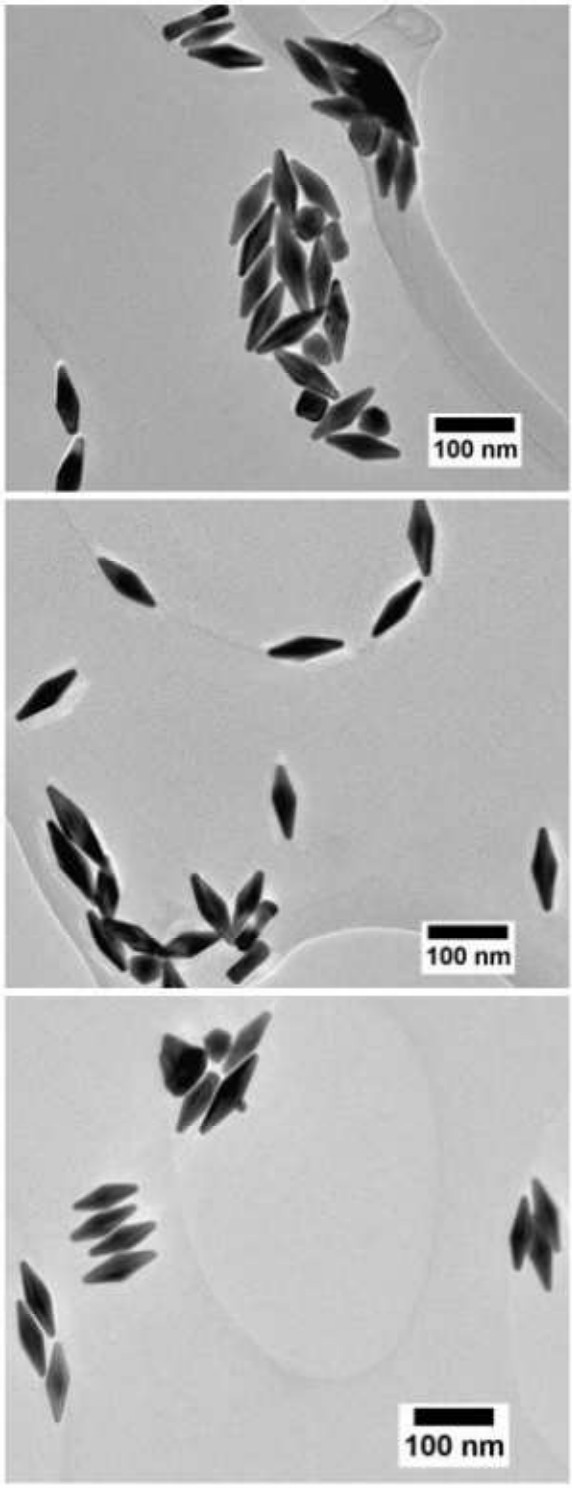

Figure S1. TEM images of gold bipyramids deposited onto the TEM grids from aqueous suspension.

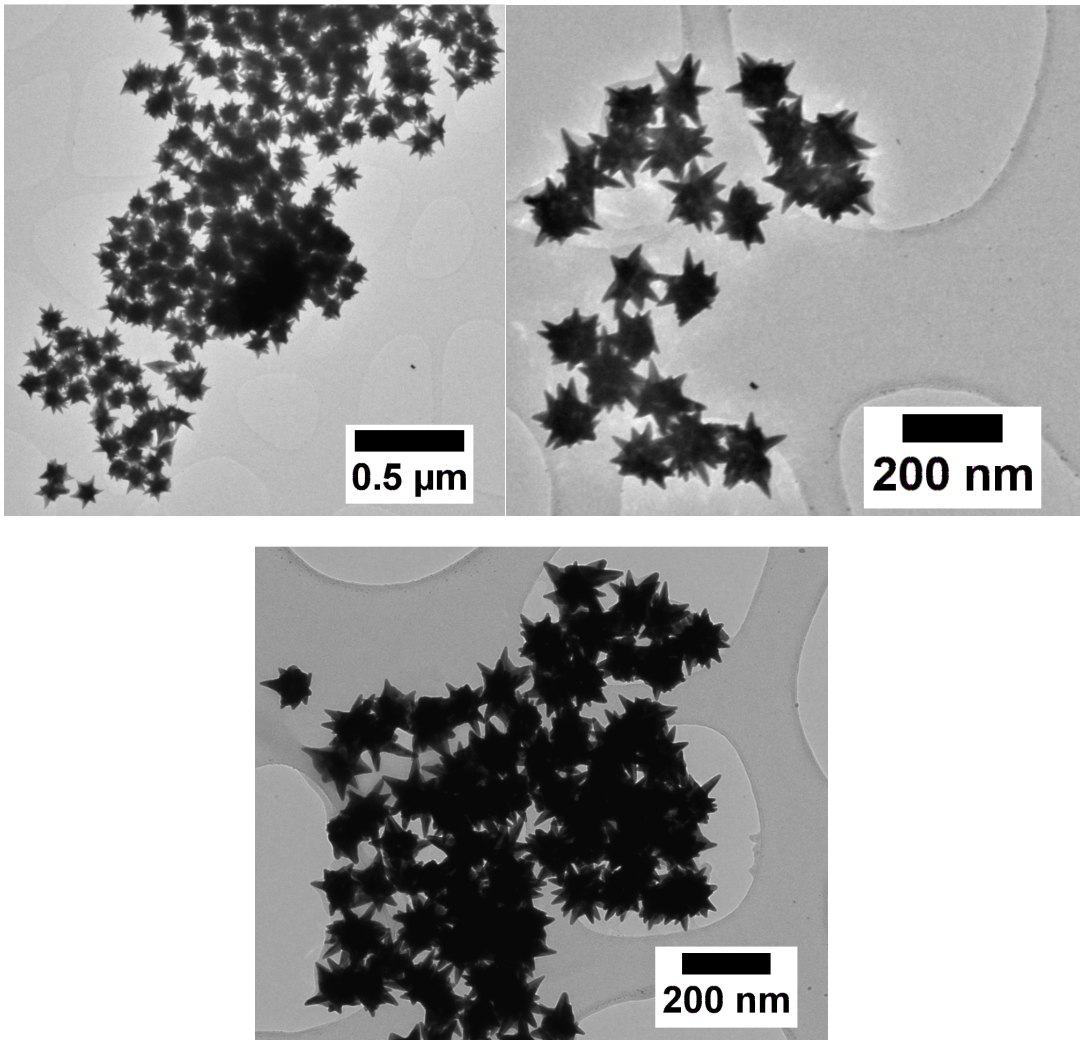

Figure S2. TEM images of gold nanostars deposited onto the TEM grids from aqueous suspension.

S1 Procedures

S1-1 Procedure for scattering measurements on bulk suspensions

The ensemble-averaged light scattering cross sections σ_{sca} of the nanoparticles in suspension were obtained by resonant light scattering (RLS) spectroscopy. The scattering cross section σ_{sca} is related to the extinction cross section σ_{ext} *via* $\sigma_{sca}(\lambda) = \varphi_{LS}(\lambda)\ \sigma_{ext}(\lambda)$ where $\varphi_{LS}(\lambda)$ is the (wavelength-dependent) scattering efficiency. This scattering efficiency $\varphi_{LS}(\lambda)$ is experimentally accessible by measuring the light scattering spectrum of the nanoparticle suspension against a scattering reference sample.

As a reference we used diluted Ludox suspension, which behaves as a perfect Rayleigh scatterer.[S1] Ludox SM30 (Aldrich) was centrifuged for 1 h at 9700 x *g*, and diluted 200 times in 0.05 M NaCl. Unprocessed scattering spectra of the samples, the reference and the solvent (water) were recorded at right angles (QE65000 spectrometer with QPOD sample compartment, Ocean Optics) under white light illumination (LS-1 light source, Ocean Optics). The (very weak) solvent background was subtracted from the recorded spectra to give the uncorrected spectra $I_{raw}(\lambda)$. These were then used to find the corrected light scattering spectra, according to Equation (S1).

$$I_{LS}(\lambda) = \lambda^{-4}\frac{I_{raw}(\lambda)}{I_{raw}^{ref}(\lambda)} \qquad \text{(S1)}$$

We work at low optical densities (A< 0.05, where A stands for absorbance) so that we can approximate the fraction of light interacting with the sample, $\mathbf{1 - 10^{-A} \approx 2.303A}$. We can then obtain the wavelength-dependent light scattering efficiency φ_{LS} from the extinction spectra and the corrected light scattering spectra (Equation (S2)).

$$\varphi_{LS}(\lambda) = \frac{I_{LS}(\lambda)}{I_{LS}^{ref}(\lambda)}\frac{A_{ref}(\lambda)}{A(\lambda)} \qquad \text{(S2)}$$

This relation holds provided that (1) the optical density is low (<0.05), (2) the reference and the sample are contained in a medium with the same refractive index (water, in our case), and (3) the reference is a perfect scatterer ($\boldsymbol{\varphi}_{\mathrm{LS}}^{\mathrm{ref}} = \mathbf{1}$ at all wavelengths).

When recalling that the corrected light scattering spectrum of the reference Rayleigh scatterer gives $\boldsymbol{I}_{\mathrm{LS}}^{\mathrm{ref}} = \boldsymbol{\lambda}^{-\mathbf{4}}$ and that its absorbance is described by $\boldsymbol{A}_{\mathrm{ref}} = \boldsymbol{p_0}\,\boldsymbol{\lambda}^{-\mathbf{4}}$, where p_0 comes from a fit of this curve to the experimental absorbance spectrum of the reference, the scattering efficiency is obtained in a simpler form shown in equation (S3), which is more robust from an experimental point of view, since the noise in the absorbance spectrum of the reference is removed by the curve fitting procedure.

$$\varphi_{\mathrm{LS}}(\lambda) = p_0 \frac{I_{\mathrm{LS}}(\lambda)}{A(\lambda)} \qquad \text{(S3)}$$

The experimental values for $\boldsymbol{\varphi}_{\mathrm{LS}}$ obtained using this method agree well with theoretical values from Mie theory for 80 nm gold spheres in water, as shown in Figure S3.

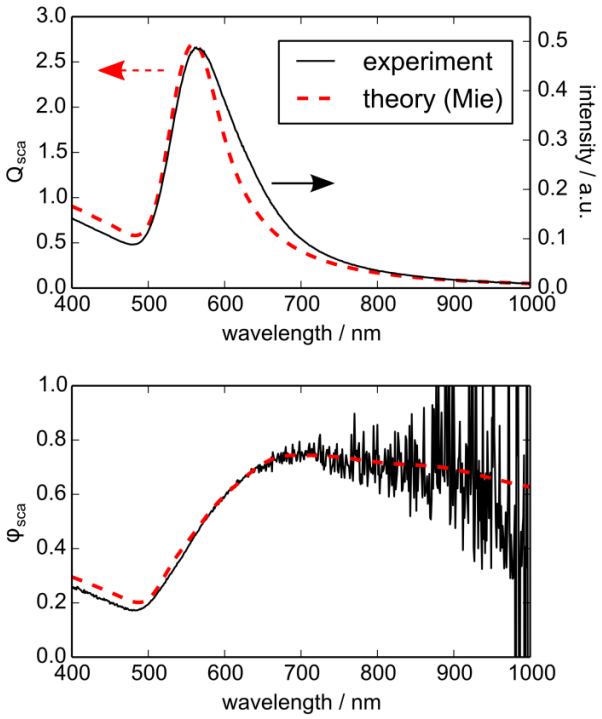

Figure S3. Comparison of experimental light scattering data (solid black lines) with results from Mie theory (dashed red lines) for 80 nm gold nanospheres in water. Top: resonant light scattering spectra. Bottom: light scattering quantum yield as a function of wavelength. The Mie calculations were carried out as described by Navarro and Werts.[S6]

The spectrum of the light scattering efficiency can be used to find the scattering cross sections via $\sigma_{sca}(\lambda) = \varphi_{LS}(\lambda)\sigma_{ext}(\lambda)$. If the concentration of the particles is known, $\sigma_{ext}(\lambda)$ is readily obtained from the absorbance spectrum. Finally we can then write equation (S4), for a 1 cm path length spectroscopic cell.

$$\sigma_{sca}(\lambda) = \frac{2303\, p_0}{c N_A} I_{LS}(\lambda) \qquad \text{(S4)}$$

Where c is the particle concentration (mol L^{-1}) and N_A Avogadro's constant. The cross sections are in cm^2. This expression emphasizes the fact that the corrected light scattering spectrum I_{LS} (Eqn. S1) has the same spectral profile as the (absolute) scattering cross section spectrum, and

would only need multiplication by a calibration constant related to the particle concentration of the sample, and the optical density of the reference.

S1-2 Experimental and burst selection procedures

The calibration procedure and the figure-of-merit of the spectrometer have been already described as well as the signal processing required for transforming the temporal light intensity signal into a luminescence spectrum.[S2] The ultimate spectral resolution is on the order of a nanometer. A binning procedure can be used to reduce noise impact in case of weak signals. The spectral range for luminescence detection is limited on the short wavelength side by the edge of a long pass filter (520 LP, Omega) used to remove the wing of the Raman signature of water which has a strong peak at about 3400 cm^{-1}.[S3]

The presence of a nanoparticle in the volume leads to the generation of a burst in the time histogram of a detection channel. Two methods for discriminating rare transient events from noise, *i.e.* methods for recognizing bursts, have been explored. The first one, on a photon-by-photon basis,[S4] was not satisfactory. The main difficulty arose from the blinking nature of the light emitted by the diffusing particle, due for instance to its Brownian rotation, which tends to divide a burst into several smaller bursts. The second method, commonly referred as “binning and thresholding”, provided satisfying and reproducible results. The selection of the bursts by this method requires two input values: a binning time and a thresholding value. Characteristic fluctuation times of the signal are obtained from fluctuation correlation spectroscopy (FCS) traces. A pertinent binning time is longer than the rotation time in order to smooth these fluctuations but not too large compared to the diffusion time so that a bin does not encompass two bursts. Consequently, the binning time was set to twice the mean diffusion time of the investigated nanoparticles. As for the thresholding value, it was implemented according to the

algorithm described by Grange *et al.*[S5] In order to prevent the overlap of two successive bursts, the chemical concentration of the nanoparticles was chosen such that, statistically, there is – on average - much less than one particle in the focal volume at the same time.

S1-3 Numerical post filtering of the fluorescent impurity

The bursts in the time-resolved trace of the luminescence intensity may be selected according to several criteria that can associate each burst to one of the luminescent species present in the sample. The simplest situation corresponds to the case where the maxima of the emission spectra of the species are sufficiently shifted apart to be unambiguously identified, with the additional constraint that the spectrum of each species does not evolve during the whole acquisition time. In this case, the bursts may be selected based upon the spectrum corresponding to each burst.

Another interesting possibility is when one species has much higher emission efficiency than the others. In this case, an intensity threshold can be applied, independently of the spectral content of each burst. Bursts are then selected based on whether their overall intensity is above the threshold. This is the criterion that we have used in the present case.

Using the threshold criterion, the initial time-resolved recording of the luminescence intensity was transformed in a set of two 'filtered' synchronous time-resolved traces of intensity. One trace only contained the recorded signal around and during the occurrence of bursts that are above threshold, the other containing the rest of the recorded signal (i.e. the bursts that are below threshold plus the noise in between bursts). Each of the traces contained gaps during the periods that the other trace is active. These gaps were filled with Poissonian noise. The filtered traces could then each be analyzed giving rise to filtered luminescence spectra and filtered correlation traces.

For the bipyramid sample, the resulting filtered luminescence spectrum of the bursts 'above threshold' is shown on Figure 7b (main text). This spectrum is entirely dominated by a nearly symmetrical band in the near-infrared spectral range (700nm-850nm), in contrast to the unfiltered spectrum, which displays a shoulder at shorter wavelengths. Analysis of the signal from the bursts 'below threshold' gives more insight into the origin of the additional signature of the short-wavelength wing. We have calculated the correlation function of this residual signal which indicated the presence of a species emitting in the visible (~ 570 nm) at a concentration in the order of a few nanomolar. This signal displays a clear time correlation, which eliminates spurious signals from the optics as the potential source.

The fit of the correlation curve indicated a translational diffusion time of 60 μs for this luminescent object, which corresponds to a hydrodynamic radius of 2.7 nm (Figure 7c, main text). This comparatively small size allows us to eliminate the possibility that the spurious short-wavelength emission results from the luminescence of spherical gold nanoparticles in the sample. Such particles would have a larger hydrodynamic radius. In a separate experiment, we have measured the luminescence decay time of the impurity species, using an optical filter to remove the contribution of the bipyramid luminescence and applying time-correlated single photon counting. The measured decay time was 2.5 ns. This is much longer than the decay times for metal nanostructure luminescence, which is on the order of tens of femtoseconds, but it is in good agreement with the value expected for a fluorescent molecule, strengthening the hypothesis of a fluorescent residual impurity, probably coming from the surfactant.

The proposed selection procedure applied to the bursts from individual nano-objects diffusing through the focal volume provides a powerful means of identifying and characterizing the contribution of several emitting species, and goes beyond what can be achieved by bulk spectroscopic techniques. Compared to other single-object techniques in which immobilized

objects are measured one at a time, correlation spectroscopy on liquid suspensions can automatically analyze large numbers of objects, and apply statistics.

The validity of this filtering procedure was confirmed by the analysis of a blank experiment with the supernatant containing only the fluorescent impurity and the analysis of a solution containing only the nanoparticles after a proper washing of the solution, with replacement by a pure surfactant to prevent aggregation.

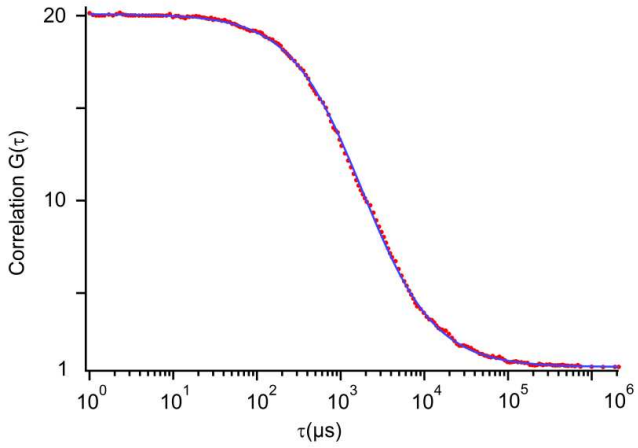

Figure S4. Correlation profile of the Rayleigh scattering of the sample of 80 nm gold nanospheres, recorded simultaneously with the photoluminescence (see Figure 3 of main text). Excitation at 430 nm (1600 μW). Red dots curve: data; Blue line: fit according to Equations 5 and 6 of main text, τ_D = 1812 μs.

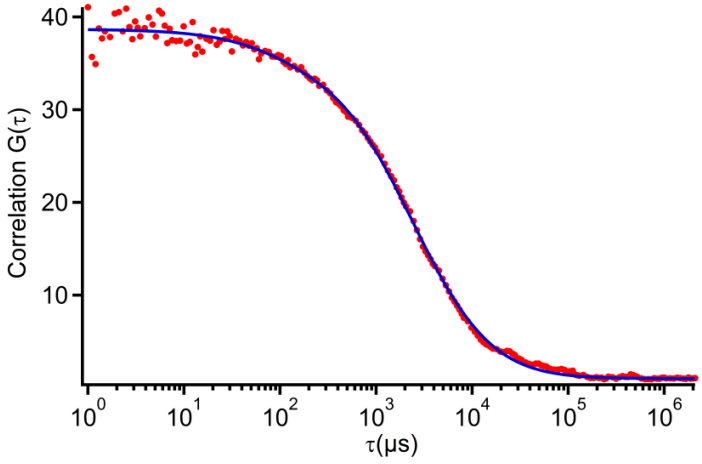

Figure S5. Correlation profile of Rayleigh scattering of gold nanostars. Red dots, experimental data; blue line, fit according to equations 5 and 6. τ_D = 2444 μs; τ_r = 79 μs; excitation wavelength 430 nm; P_{exc} = 1400 μW.

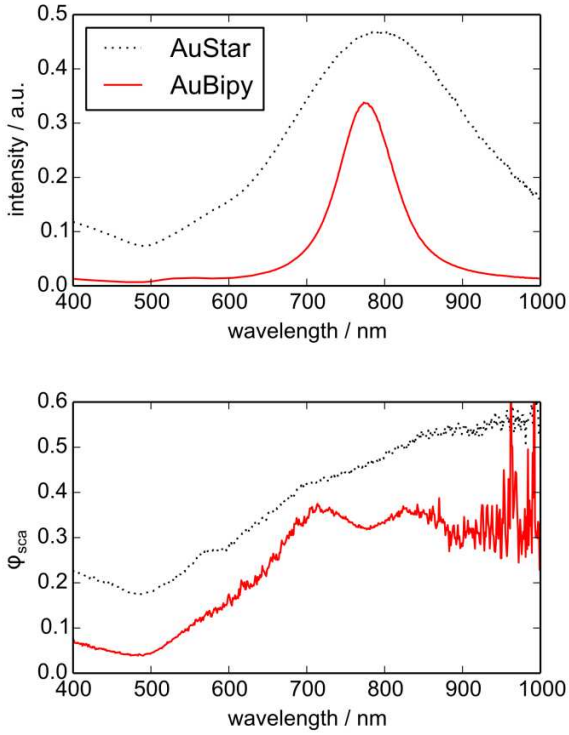

Figure S6. Resonant light scattering by gold nanostars (AuStar, black dotted lines) and gold bipyramids (AuBipy, red solid lines) in aqueous suspension. Top: corrected light scattering spectra. Bottom: light scattering "quantum yield" (see ref S6) as a function of wavelength.

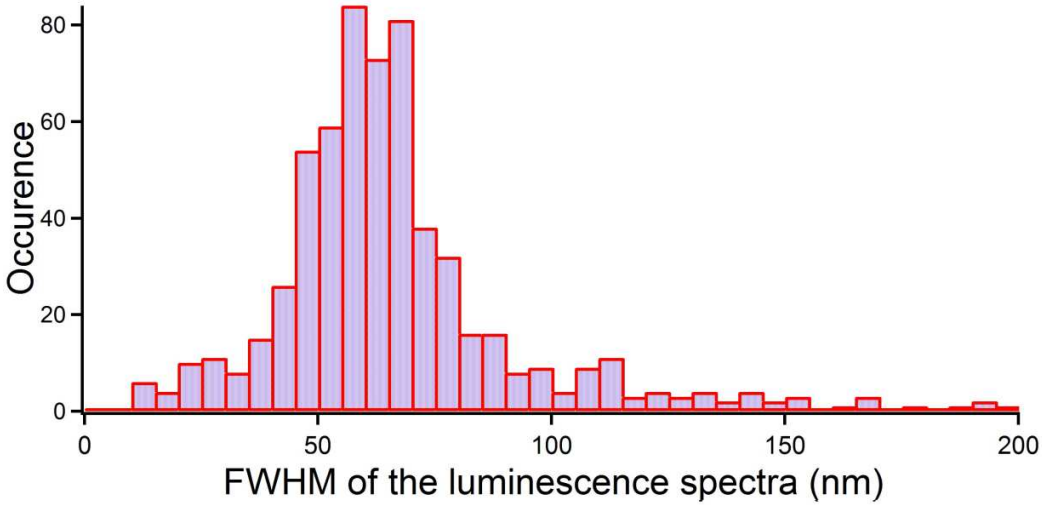

Figure S7. Histogram of the widths (FWHM) of the luminescence spectra of single gold nanobipyramids freely diffusing in water. This curve is extracted from the same data as Figure 8 in the main text.

REFERENCES

(S1) G. Deželić and J. P. Kratohvil, *Kolloid-Z*, 1960, **173**, 38–48.

(S2) M. Loumaigne, P. Vasanthakumar, A. Richard and A. Débarre, *ACS Nano*, 2012, **6**, 10512–23.

(S3) B. M. Auer and J. L. Skinner, *J. Chem. Phys.*, 2008, **128**, 224511.

(S4) K. Zhang and H. Yang, *J. Phys. Chem. B*, 2005, **109**, 21930–7.

(S5) W. Grange, P. Haas, A. Wild, M. A. Lieb, M. Calame, M. Hegner and B. Hecht, *J. Phys. Chem. B*, 2008, **112**, 7140–4.

(S6) J. R. G. Navarro and M. H. V. Werts, *Analyst,* **2013**, *138*, 583–592.